Parametric stiffness analysis of the Orthoglide

Félix Majou[1,2], Clément Gosselin[2], Philippe Wenger[1] and Damien Chablat[1]

[1] *IRCCyN* *, *1 rue de la Noë, 44321 Nantes, France*
[2] *Département de Génie Mécanique, Université Laval, Québec, Canada, G1K 7P4*

1$^{\text{er}}$ février 2008

Abstract

This paper presents a parametric stiffness analysis of the Orthoglide, a 3-DOF translational Parallel Kinematic Machine. First, a compliant modeling of the Orthoglide is conducted based on an existing method. Then stiffness matrix is symbolically computed. This allows one to easily study the influence of the geometric design parameters on the matrix elements. Critical links are displayed. Cutting forces are then modeled so that static displacements of the Orthoglide tool during slot milling are symbolically computed. Influence of the geometric design parameters on the static displacements is checked as well. Other machining operations can be modeled. This parametric stiffness analysis can be applied to any parallel manipulator for which stiffness is a critical issue.

Keywords : Parallel Kinematic Machine ; Stiffness ; Parametric analysis ;

1 Introduction

Parallel manipulators are claimed to offer good stiffness and accuracy properties, as well as good dynamic performances. This makes them attractive for innovative machine-tool structures for high speed machining [1], [2], [3]. When a parallel manipulator is intended to become a Parallel Kinematic Machine (PKM), stiffness becomes a very important issue in its design [4], [5], [6]. In this paper is presented a parametric stiffness analysis of the Orthoglide, a 3-axis translational PKM prototype developped at IRCCyN [7].

One of the first stiffness analysis methods for parallel mechanisms is based on a kinetostatic modeling [8]. It proposes to map the stiffness of parallel mechanisms by taking into account the compliance of the actuated joints. This method is not appropriate for PKM whose legs, unlike hexapods, are subject to bending [9]. In [10], a stiffness estimation of a tripod-based PKM is proposed that solves this problem. However the stiffness model presented is not general enough. This gap is filled in [11]. The method is based on a flexible-link lumped parameter model that replaces the compliance of the links by localized virtual compliant joints and rigid links. The approach has two differences from that presented in [10] (i), the way the link compliances are modeled (ii), the equations allowing the computation of the stiffness model, that are more general.

This method is applied to the Orthoglide for a parametric stiffness analysis. The stiffness matrix elements are symbolically computed. This allows an easy analysis of the influence of the Orthoglide critical design parameters. No numerical computations are conducted until graphical results are generated. First we present the Orthoglide, then the compliant model. The results showing the influence of the parameters are presented next.

2 Compliant modeling of the Orthoglide

2.1 Kinematic architecture of the Orthoglide

The Orthoglide is a translational 3-axis PKM prototype designed for machining applications. The mobile platform is connected to three orthogonal linear drives through three identical RP_aR serial chains (where R

1

stands for Revolute and P_a for Parallelogram) (Fig.1), and it moves in the Cartesian workspace while maintaining a fixed orientation. The Orthoglide is optimized for a prescribed workspace with prescribed kinetostatic performances. Its kinematic analysis, design and optimization are fully described in [12].
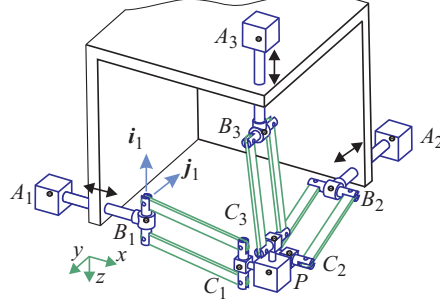

FIG. 1 – The Orthoglide kinematic architecture

2.2 Parameters for compliant modeling

The parameters used for the compliant modeling of the Orthoglide are presented in Figure 2 and in Table 1. These parameters correspond to a "beam-like" modeling of the Orthoglide legs. The foot has been designed to prevent each parallelogram from colliding with the corresponding linear motion guide.
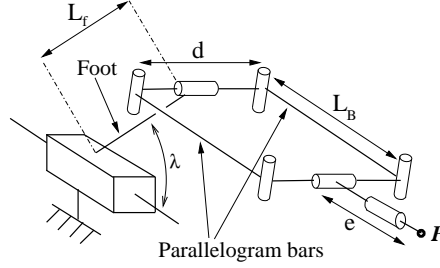

FIG. 2 – Leg geometrical parameters

Parameter	Description
L_f	Foot length, see Fig.2
h_f, b_f	Foot section sides
$I_{f_1} = b_f.h_f^3/12$	Foot section moment of inertia 1
$I_{f_2} = h_f.b_f^3/12$	Foot section moment of inertia 2
d	Distance between parallelogram bars, see Fig.2
L_B	Parallelogram bar length, see Fig.2
S_B	Parellelogram bar cross-section area

TAB. 1 – Geometric parameters

2.3 Compliant modeling with flexible links

In the lumped model described in [13], the leg links are considered as flexible beams and are replaced by rigid beams mounted on revolute joints plus torsional springs located at the joints (Fig. 3).

From deriving the relationship between the force F and the deformation $y(x)$, the local torsional stiffness k can be computed :
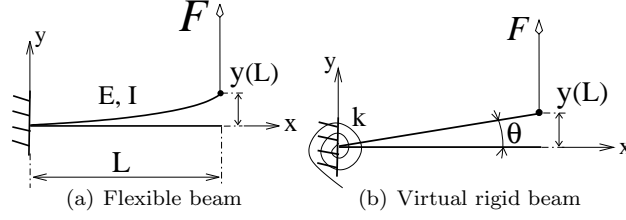
$$EIy''(x) = F(L-x)$$

2

(a) Flexible beam   (b) Virtual rigid beam

FIG. 3 – General model for flexible link

$$
\vdots
$$

$$
\begin{aligned}
EIy(L) &= FL^3/3 \\
\to \theta \simeq y(L)/L &= FL^2/3EI \\
k &= FL/\theta \\
\to k &= 3EI/L
\end{aligned}
$$

If the Orthoglide leg actuator is locked, then one leg can withstand one force F and one torque T (Fig. 4), that are transmitted along the parallelogram bars and the foot. For a compliant modeling that uses virtual compliant joints, it is important to understand how external forces are transmitted, and what their effect on the leg links is.
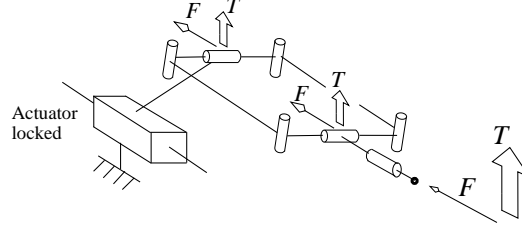

FIG. 4 – Forces transmitted in a leg

Three virtual compliant joints are modeled along the Orthoglide leg. They are described in Table 2. The determination of the virtual joint stiffnesses is not detailed here to save space. Since the actuator is assumed to be much stiffer than the virtual compliant joints, it is not included in foot stiffnesses. The leg links compliances modeled in Table 2 were selected beforehand as the most significant. The joint compliances are not taken into account in our model.

3   Symbolic computing of the Orthoglide stiffness matrix

The virtual compliant joints stiffnesses depend on the design parameters. In this section, symbolic expressions of stiffness matrix elements are symbolically computed. This part is based on a stiffness model that was fully described in [11]. Therefore, the description of the model will only be summarized here. Fig. 5 represents the lumped model of a leg with flexible links.

The Jacobian matrix $\mathbf{J}_i$ of the ith leg of the Orthoglide is obtained from the Denavit-Hartenberg parameters of the ith leg with flexible links. This matrix maps all leg joint rates (including the virtual compliant joints) into the generalized velocity of the platform, i.e.,

$$
\mathbf{J}_i \dot{\theta}_i = \mathbf{t}
$$

where
$$
\dot{\theta}_i^T = \begin{bmatrix} \dot{\theta}_{i_1} & \dot{\theta}_{i_2} & \dot{\theta}_{i_3} & \dot{\theta}_{i_4} & \dot{\theta}_{i_5} & \dot{\theta}_{i_6} & \dot{\theta}_{i_7} & \dot{\theta}_{i_8} \end{bmatrix}
$$
is the vector containing the 8 actuated, passive and compliant joint rates of leg i, $\mathbf{t}$ is the twist of the platform. The P_a joint parameterization imposes $\dot{\theta}_{i_5} = -\dot{\theta}_{i_{5bis}}$, which makes $\dot{\theta}_{i_5}$ and $\dot{\theta}_{i_{5bis}}$ dependent. $\dot{\theta}_{i_5}$ is chosen to

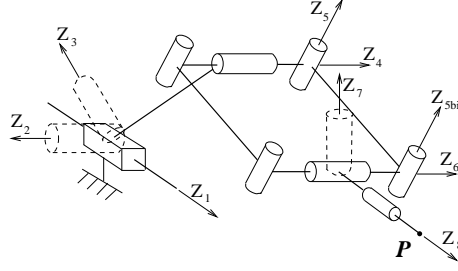| Stiffness and description	Figure
k_{act} : translational stiffness of the prismatic actuator	
$2EI_{f_2}/L_f$: foot bending due to torque T	
$3EI_{f_1}/L_f$: foot bending due to force F	
$ES_B d^2/2L_B$: differential tension of parallelogram bars due to torque T	

TAB. 2 – Virtual compliant joints modeling

FIG. 5 – Flexible leg

model the circular translational motion, and finally $\mathbf{J}_i$ is written as

$$\mathbf{J}_i = \left[\begin{array}{cccc} 0 & \mathbf{e}_{i_2} & \mathbf{e}_{i_3} & \mathbf{e}_{i_4} \\ \mathbf{e}_{i_1} & \mathbf{e}_{i_2} \times \mathbf{r}_{i_2} & \mathbf{e}_{i_3} \times \mathbf{r}_{i_3} & \mathbf{e}_{i_4} \times \mathbf{r}_{i_4} \end{array} \right.$$

$$\left. \begin{array}{cccc} 0 & \mathbf{e}_{i_6} & \mathbf{e}_{i_7} & \mathbf{e}_{i_8} \\ \mathbf{e}_{i_5} \times \mathbf{r}_{i_5} - \mathbf{e}_{i_{5bis}} \times \mathbf{r}_{i_{5bis}} & \mathbf{e}_{i_6} \times \mathbf{r}_{i_6} & \mathbf{e}_{i_7} \times \mathbf{r}_{i_7} & \mathbf{e}_{i_8} \times \mathbf{r}_{i_8} \end{array} \right]$$

in which $\mathbf{e}_{i_j}$ is the unit vector along joint j of leg i and $\mathbf{r}_{i_j}$ is the vector connecting joint j of leg i to the platform reference point. Therefore the Jacobian matrix of the Orthoglide can be written as :

$$\mathbf{J} = \left[\begin{array}{ccc} \mathbf{J}_1 & 0 & 0 \\ 0 & \mathbf{J}_2 & 0 \\ 0 & 0 & \mathbf{J}_3 \end{array} \right]$$

One then has :

$$\mathbf{J}\dot{\theta} = \mathbf{R}\mathbf{t} \qquad (1)$$

4

$$\text{with} \quad \mathbf{R} = \begin{bmatrix} I_6 \\ I_6 \\ I_6 \end{bmatrix}^T \quad \text{and} \quad \mathbf{t} = \left\{ \begin{matrix} \Omega \\ \mathbf{V} \end{matrix} \right\}$$

$\dot{\theta}$ being the vector of the 24 joint rates, that is $\dot{\theta} = \begin{bmatrix} \dot{\theta}_1^T & \dot{\theta}_2^T & \dot{\theta}_3^T \end{bmatrix}$. Unactuated joints are then eliminated by writing the geometric conditions that constrain the two independent closed-loop kinematic chains of the Orthoglide kinematic structure :

$$\mathbf{J}_1 \dot{\theta}_1 = \mathbf{J}_2 \dot{\theta}_2 \tag{2}$$

$$\mathbf{J}_1 \dot{\theta}_1 = \mathbf{J}_3 \dot{\theta}_3 \tag{3}$$

From (2) and (3) one can obtain (see [11] for details) :

$$\mathbf{A}\dot{\theta}' = \mathbf{B}\dot{\theta}''$$

where $\dot{\theta}'$ is the vector of joint rates without passive joints and $\dot{\theta}''$ is the vector of joint rates with only passive joints. Hence :

$$\dot{\theta}'' = \mathbf{B}^{-1}\mathbf{A}\dot{\theta}'$$

Then a matrix $\mathbf{V}$ is obtained (see [11] for details) such that :

$$\dot{\theta} = \mathbf{V}\dot{\theta}' \tag{4}$$

From (1) and (4) one can obtain :

$$\mathbf{JV}\dot{\theta}' = \mathbf{Rt} \tag{5}$$

As matrix $\mathbf{R}$ represents a system of 18 compatible linear equations in 6 unknowns, one can use the least-square solution to obtain an exact solution from (5) :

$$\mathbf{t} = (\mathbf{R}^T\mathbf{R})^{-1}\mathbf{R}^T\mathbf{JV}\dot{\theta}'$$

Now let $\mathbf{J}'$ be represented as :

$$\mathbf{J}' = (\mathbf{R}^T\mathbf{R})^{-1}\mathbf{R}^T\mathbf{JV}$$

Then one has :

$$\mathbf{t} = \mathbf{J}'\dot{\theta}' \tag{6}$$

According to the principle of virtual work, one has :

$$\tau^T \dot{\theta}' = \mathbf{w}^T\mathbf{t} \tag{7}$$

where τ is the vector of forces and torques applied at each actuated or virtual compliant joint and $\mathbf{w}$ is the external wrench applied at the end effector, point $\boldsymbol{P}$. Gravitational forces are neglected. By substuting (6) in (7), one can obtain :

$$\tau = \mathbf{J}'^T\mathbf{w} \tag{8}$$

The forces and displacements of each actuated or virtual compliant joint can be related by Hooke's law, that is for the whole structure one has :

$$\tau = \mathbf{K}_J \Delta\theta' \tag{9}$$

with :

$$\mathbf{K}_J = \begin{bmatrix} \mathbf{A} & 0 & 0 \\ 0 & \mathbf{A} & 0 \\ 0 & 0 & \mathbf{A} \end{bmatrix}$$

5

and :

$$\mathbf{A} = \begin{bmatrix} k_{act} & 0 & 0 & 0 \\ 0 & \frac{3EI_{f_1}}{L_f} & 0 & 0 \\ 0 & 0 & \frac{2EI_{f_2}}{L_f} & 0 \\ 0 & 0 & 0 & \frac{ES_B d^2}{L_B} \end{bmatrix} \tag{10}$$

$\Delta\theta'$ only includes the actuated and virtual compliant joints, that is by equating (8) with (9) :

$$\mathbf{K}_J \Delta\theta' = \mathbf{J'}^T \mathbf{w}$$

hence :

$$\Delta\theta' = \mathbf{K}_J^{-1} \mathbf{J'}^T \mathbf{w}$$

Pre-multiplying both sides by $\mathbf{J'}$ one obtains :

$$\mathbf{J'}\Delta\theta' = \mathbf{J'}\mathbf{K}_J^{-1} \mathbf{J'}^T \mathbf{w} \tag{11}$$

Substituting (6) into (11), one obtains :

$$\mathbf{t} = \mathbf{J'}\mathbf{K}_J^{-1} \mathbf{J'}^T \mathbf{w}$$

Finally the compliance matrix κ is obtained as follows :

$$\kappa = \mathbf{J'}\mathbf{K}_J^{-1} \mathbf{J'}^T$$

In the Orthoglide case we obtain a simplified compliance matrix :

$$\kappa = \begin{pmatrix} \kappa_{11} & 0 & 0 & 0 & \kappa_{15} & \kappa_{15} \\ 0 & \kappa_{11} & 0 & \kappa_{24} & 0 & \kappa_{26} \\ 0 & 0 & \kappa_{11} & 0 & \kappa_{35} & 0 \\ 0 & \kappa_{24} & 0 & \kappa_{44} & 0 & \kappa_{46} \\ \kappa_{15} & 0 & \kappa_{35} & 0 & \kappa_{55} & 0 \\ \kappa_{15} & \kappa_{26} & 0 & \kappa_{46} & 0 & \kappa_{66} \end{pmatrix} \tag{12}$$

And the Cartesian stiffness matrix is :

$$\mathbf{K} = \mathbf{J'}\mathbf{K}_J^{-1} \mathbf{J'}^{T^{-1}}$$

Remarks :

From the expression of matrix $\mathbf{A}$ (see eq. 10) we deduce that all elements of stiffness matrix $\mathbf{K}$ can be factored either in factors of E or in factors of k_{act}. As k_{act} is assumed infinite compared to other stiffnesses, the elements of $\mathbf{K}$ which are factors of k_{act} must be eliminated. Also obviously when E increases, $\mathbf{K}$ elements increase too, which is in accordance with intuition. Young's modulus E should then be eliminated from $\mathbf{K}$ elements expressions because its influence needs no further study.

In eq. (12) one should notice that $\kappa_{11} = \kappa_{22} = \kappa_{33}$, and $\kappa_{15} = \kappa_{16}$. Also, we noticed that when X=Y=Z we have $\kappa_{44} = \kappa_{55} = \kappa_{66}$.

4   Parametric stiffness analysis

In this part, we study the in uence of the geometric parameters on the elements of the Orthoglide stiffness matrix. For a realistic inspection of the symbolic expressions of these elements, it is necessary to replace some parameters by numerical values, once the symbolic expressions have been obtained. Numerical values of the design parameters come from the Orthoglide prototype [14].

4.1 Qualitative analysis at the isotropic configuration

There is an isotropic configuration in the Orthoglide workspace [7]. This configuration gives a good insight of the Orthoglide general performances. It happens when the tool point P is at the intersection of the three actuated joint axes (see Fig. 1). In this configuration, the stiffness matrix $\mathbf{K}$ is diagonal and the symbolic expressions of its elements are simplified :

$$
K = E/2 \begin{pmatrix} K_a & 1 & 1 & 1 & 1 & 1 \\ 1 & K_a & 1 & 1 & 1 & 1 \\ 1 & 1 & K_a & 1 & 1 & 1 \\ 1 & 1 & 1 & K_b & 1 & 1 \\ 1 & 1 & 1 & 1 & K_b & 1 \\ 1 & 1 & 1 & 1 & 1 & K_b \end{pmatrix}
$$

$E = 2K_a$ being the torsional stiffness with

$$
Ka = \left(\frac{LB}{d^2 S_B} + \frac{3L f cos^2 \lambda}{h_f b_f^3} \right)^{-1} \tag{13}
$$

and $E = 2K_b$ being the translational stiffness with

$$
Kb = \left(\frac{0.5 h_f^3 b_f}{L_f^3 (1 - cos^2 \lambda)} + \frac{E}{2 k_{act}} \right)^{-1} \tag{14}
$$

– From the inspection of K_a we note that increasing the cross-section areas SB and $b_f h_f$ increases the torsional stiffness, which is in accordance with intuition. Increasing the distance d between the parallelogram bars increases the torsional stiffness. Also, it is no surprise that increasing L_f or L_B decreases the torsional stiffness. It is no surprise that K_a and K_b increase when E increases, and that K_b increases when k_{act} increases, while Ka does not depend on k_{act}, the prismatic actuated joint stiffness. K_a and K_b do not depend on e at the isotropic configuration.
– From the inspection of K_b we note that increasing the cross-section area $b_f h_f$ increases the translational stiffness, as increasing the foot length L_f does. We also note that if λ (angle between the foot and the actuated joint axis) decreases toward zero, then the translational stiffness tends toward infinite. This is in accordance with intuition since at the isotropic configuration, if $\lambda = 0$ then the virtual compliant joint "foot bending due to force F" (see Tab. 2) is not requested because the applied force axis crosses the virtual compliant joint axis.
Furthermore, if $\lambda = 0$, the cantilever disappears. As this cantilever is aimed at preventing each parallelogram from colliding with the corresponding linear motion guide, from a designer point of view the conclusion could be : "λ should be lowered to increase the translational stiffness, but there should remain enough cantilever for the workspace volume to be large enough".

4.2 Quantitative analysis at the isotropic configuration
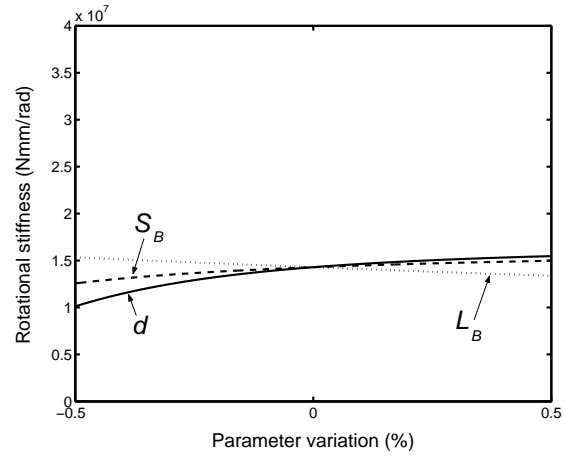
The qualitative analysis conducted above provides an interesting insight of the influence of the geometrical parameters on rotational and translational stiffnesses. Quantitative information is now obtained by studying the influence on K_a and K_b of a $+/-50\%$ variation of the numerical value of each design parameter. The results are shown on Fig.6 and on Fig.7. From Fig. 6 analysis, we can go further than the qualitative analysis and see that d, S_B and L_B have very little influence on the rotational stiffness while L_f , h_f b_f and λ have much more influence. From Fig. 7 we note, as deduced from the qualitative analysis, that decreasing L_f or λ increases the translational stiffness, and that increasing hf can improve the translational stiffness. Increasing hf does not reduce the workspace volume like reducing L_f does. However increasing hf increases the foot weight, which could be prejudicial to the dynamic performances. The proof of this forecast needs further investigations. Quantitative analysis provides another point of view and helps in a better understanding of the influence of the geometric design parameters on the machine stiffness.

5 Conclusions

A parametric stiffness analysis of a 3-axis PKM prototype, the Orthoglide, was conducted. First, a compliant model of the Orthoglide was obtained, then an existing stiffness analysis method for parallel manipulators
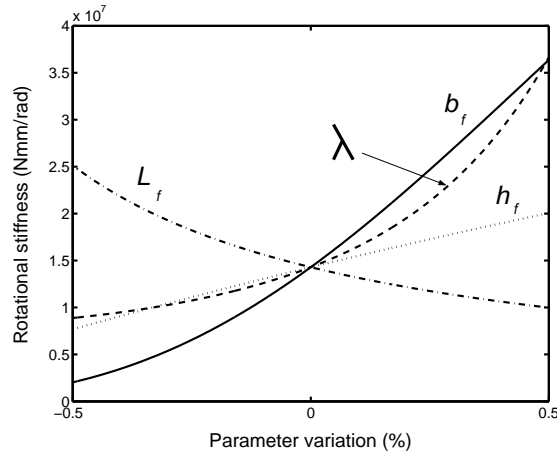
(a) Influence of L_f , b_f , h_f and λ (b) Influence of d, L_B and S_B

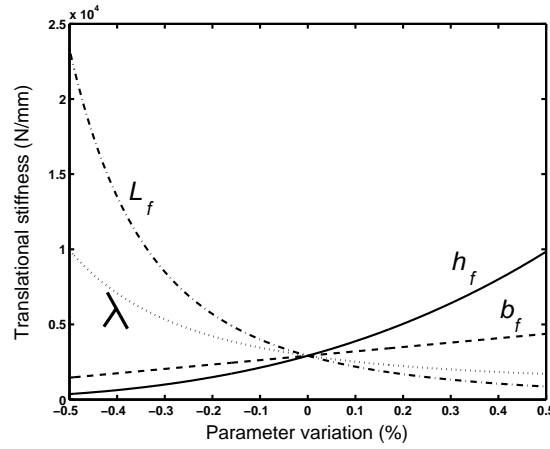FIG. 6 – Quantitative influence of the geometric parameters on the rotational stiffness $E = 2K_a$

FIG. 7 – Quantitative influence of the geometric parameters h_f , b_f , L_f and d on the translational stiffness $E = 2K_b$

was applied to the Orthoglide. The stiffness matrix elements were computed symbolically. In the isotropic configuration, the influence of the geometric design parameters on the rotational and translational stiffnesses was studied through qualitative and quantitative analyses. These provided relevant information for stiffness-oriented design or optimization of the Orthoglide.

This example of a parametric stiffness analysis shows that simple symbolic expressions carefully built and interpreted provide broad information on parallel manipulators stiffness features. Comparison of the stiffness model with a finite elements model and with stiffness tests on the prototype are currently being conducted.

Références

[1] J. Tlusty, J. Ziegert, S. Ridgeway, *Fundamental Comparison of the Use of Serial and Parallel Kinematics for Machine Tools*, Annals of the CIRP, vol. 48., no. 1, 1999.

[2] P. Wenger, C. M. Gosselin, B. Maillé, *A Comparative Study of Serial and Parallel Mechanism Topologies for Machine Tools*, PKM'99, pp 23-32, Milano, 1999.

[3] F. Majou, P. Wenger, D. Chablat, *The design of Parallel Kinematic Machine Tools using Kinetostatic Performance Criteria*, 3rd International Conference on Metal Cutting and High Speed Machining, Metz, France, June 2001.

[4] G. Pritschow, K.-H. Wurst, *Systematic Design of Hexapods and Other Parallel Link Systems*, Annals of the CIRP, vol. 46, no. 1, pp 291-295, 1997.

[5] O. Company, F. Pierrot, *Modelling and Design Issues of a 3-axis Parallel Machine-Tool*, Mechanism and Machine Theory, vol. 37, pp 1325-1345, 2002.

[6] T. Brogardh, *PKM Research - Important Issues, as seen from a Product Development Perspective at ABB Robotics*, Workshop on Fundamental Issues and Future Research Directions for Parallel Mechanisms and Manipulators, Quebec City, Canada, October 2002.

[7] P. Wenger, D. Chablat, *Kinematic Analysis of a New Parallel Machine Tool*, 7th International Symposium on Advances in Robot Kinematics, Piran-Portoroz, Slovenia, June 2000.

[8] C. M. Gosselin, *Stiffness Mapping for Parallel Manipulators*, IEEE Transactions on Robotics and Automation, vol. 6, pp 377-382, June 1990.

[9] X. Kong, C. M. Gosselin, *Kinematics and Singularity Analysis of a Novel Type of 3-CRR 3-DOF Translational Parallel Manipulator*, The International Journal of Robotics Research, vol. 21, no. 9, pp. 791–798, September 2002.

[10] T. Huang, X. Zhao, D. J. Whitehouse, *Stiffness Estimation of a Tripod-based Parallel Kinematic Machine*, IEEE Transactions on Robotics and Automation, vol. 18, no. 1, pp 50-58, February 2002.

[11] C. M. Gosselin, D. Zhang, *Stiffness Analysis of Parallel Mechanisms using a Lumped Model*, International Journal of Robotics and Automation, vol. 17, no. 1, pp 17-27, 2002.

[12] D. Chablat and P. Wenger, *Architecture Optimization of the Orthoglide, a 3-DOF Parallel Mechanism for Machining Applications*, IEEE Transactions on Robotics and Automation, vol. 19, no. 3, pp 403-410, June 2003.

[13] D. Zhang, *Kinetostatic Analysis and Optimization of Parallel and Hybrid Architectures for Machine Tools*, Ph.D Thesis, Université Laval, April 2000.

[14] www.irccyn.ecnantes.fr/ wenger/Orthoglide, Orthoglide, Web site, June 2002.